Mahesh H. Mankani, MD
Sergei A. Kuznetsov, PhD
Nilo A. Avila, MD
Albert Kingman, PhD
Pamela Gehron Robey, PhD

Index terms:
Animals
Bone marrow, transplantation
Bones, CT, 40.12119
Computed tomography (CT), quantitative, 40.12119
Hydroxyapatite
Phantoms

Published online
10.1148/radiol.2302011529
Radiology 2004; 230:369–376

Abbreviations:
BMD = bone mineral density
HA-TCP = hydroxyapatite–tricalcium phosphate
ROC = receiver operating characteristic

[1] From the Division of Plastic Surgery, Department of Surgery, University of California–San Francisco, San Francisco General Hospital, 1001 Potrero Ave, Ward 3A, San Francisco, CA 94110 (M.H.M.); Craniofacial and Skeletal Diseases Branch (S.A.K., P.G.R.) and Biostatistics Core, Office of the Director (A.K.), National Institute of Dental and Craniofacial Research, National Institutes of Health, Bethesda, Md; Department of Radiology, Clinical Center, National Institutes of Health, Bethesda, Md (N.A.A.). Received September 14, 2001; revision requested October 23; final revision received May 23, 2003; accepted June 18. **Address correspondence to** M.H.M. (e-mail: *mmankani@sfghsurg.ucsf.edu*).

Author contributions:
Guarantor of integrity of entire study, M.H.M.; study concepts and design, M.H.M.; literature research, M.H.M.; clinical and experimental studies, M.H.M., S.A.K.; data acquisition, M.H.M., S.A.K., N.A.A.; data analysis/interpretation, all authors; statistical analysis, M.H.M., A.K.; manuscript preparation, definition of intellectual content, editing, revision/review, and final version approval, all authors

Bone Formation in Transplants of Human Bone Marrow Stromal Cells and Hydroxyapatite–Tricalcium Phosphate: Prediction with Quantitative CT in Mice[1]

PURPOSE: To determine whether quantitative computed tomography (CT) can be used to estimate the extent of new bone formation in hydroxyapatite–tricalcium phosphate (HA-TCP)–based transplants.

MATERIALS AND METHODS: Bone-forming transplants were generated by attaching cultured human bone marrow stromal cells to aliquots of HA-TCP particles and were placed in subcutaneous pockets in immunocompromised mice. After 8 weeks, the transplants were individually imaged; each scan included a phantom. Overall bone mineral density (BMD) of each transplant was obtained. Hematoxylin-eosin–stained sections of the same transplants were then examined histologically, which is the reference standard for assessing bone formation. The extent of bone in each transplant was scored on a semiquantitative scale ranging from 0 to 4 by three independent blinded observers; the bone score for each transplant was calculated by averaging the three observer scores. BMD was compared with the histologically determined bone score for each transplant. Statistical evaluations included *(a)* calculation of empiric receiver operating characteristic curves to determine optimum BMD thresholds and *(b)* determination of the relationship between BMD and bone score, including derivation of Pearson correlation coefficients.

RESULTS: One hundred twenty transplants were evaluated. Average BMD of 600 mg/cm^3 K_2HPO_4 or more was noted in transplants with appreciable bone formation (bone score $\geq$ 3), while average BMD of less than 600 mg/cm^3 K_2HPO_4 was seen in transplants with poor bone formation (bone score < 3) ($P < .001$). Among transplants with appreciable bone formation, the BMD was proportional to the extent of mineralized matrix present in the new bone.

CONCLUSION: Use of quantitative CT offers a practical approach for the noninvasive determination of new bone formation in mineralizing bone marrow stromal cells and HA-TCP transplants.

Transplantation of bone graft extenders, which can reduce the amount of bone graft needed to complete a reconstruction, or bone graft replacements, such as osteoconductive matrices, have gained considerable interest during the past few years. In lieu of or in addition to bone autografts or allografts, surgeons have reconstructed bone defects with materials that contain hydroxyapatite–tricalcium phosphate (HA-TCP) (1–12). However, of great concern to reconstructive surgeons is the current lack of a reliable noninvasive modality for the evaluation of new bone formation in the presence of these mineral-containing matrices, since the extent of bone formation and therefore graft success is uncertain (6,13–15). HA-TCP has a high density, comparable to that of cortical bone. On both radiographs and standard computed tomographic (CT) images, HA-TCP transplants that have no associated bone formation are indistinguishable from HA-TCP transplants that do have associated bone formation (Mankani MH, Kuznetsov SA, Robey PG, unpublished data, 2000). Yet CT offers an advantage over radiography. With CT, the density of a volume of tissue can be accurately measured with quantitative CT techniques and software (16–21). We hypothesized that the bone mineral density (BMD) of HA-TCP transplants may vary by the quantity of bone that they contain. Thus, the purpose of our study was to determine whether quantitative CT can be used to estimate the extent of new bone formation in HA-TCP–based transplants.

MATERIALS AND METHODS

Cell Culture and Transplant Preparation

Surgical specimens were obtained with either fragments of normal unaffected bone with bone marrow from patients undergoing reconstructive surgery or diseased bone from patients undergoing diagnostic bone biopsies. Diagnoses included fibrous dysplasia of bone, McCune-Albright syndrome, aplastic anemia, and myelodysplasia. These specimens represented all that were collected during the duration of the study. Tissue procurement proceeded in accordance with institutional regulations governing the use of human subjects, including the use of informed consent. Multicolony strains of bone marrow stromal cells were derived from the bone marrow in a manner previously described (22). Briefly, a single cell suspension of bone marrow cells was cultured in growth medium consisting of α Eagle minimum essential medium, 2 mmol/L L-glutamine, 100 U/mL penicillin, 100 μg/mL streptomycin sulfate, 10^{-8} mol/L dexamethasone, 10^{-4} mol/L L-ascorbic acid phosphate magnesium salt n-hydrate, and 20% fetal bovine serum of a preselected lot. After 2 hours, nonadherent cells were removed by means of extensive washing. The cells were then incubated at 37°C in an atmosphere of 100% humidity and 5% CO_2.

Upon reaching confluence, cells were trypsin released and pipetted into 1.8-mL polypropylene screw-cap vials (CryoTubes; Nalge Nunc International, Rochester, NY), each previously loaded with a 40-mg aliquot of HA-TCP particles (Zimmer; Warsaw, Ind). With use of a sieve shaker (CSC Scientific, Fairfax, Va), only particles 0.5–1.0 mm in diameter were isolated and used. These represented the specific size and shape that were commercially available (Collagraft; Zimmer), which is approved by the U.S. Food and Drug Administration. Each tube received 1.2×10^6 to 3.4×10^6 cells (passages 2–5). The mixtures were incubated for 90 minutes at 37°C on a slowly rotating platform. They were then centrifuged at 200*g* for 60 seconds, and the supernatant was discarded.

Thirty-two 3-month-old immunocompromised female mice (Bg-Nu-Xid; Harlan-Sprague-Dawley, Indianapolis, Ind) served as transplant recipients. All animals were cared for according to the policies and principles established by the Animal Welfare Act and the National Institutes of Health Guide for the Care and Use of Laboratory Animals. Surgical procedures were performed in accordance with specifications of an approved institutional small animal protocol. Mice were anesthetized with a combination of intraperitoneal ketamine (Ketaset; Fort Dodge Animal Health, Overland Park, Kan) (140 mg per kilogram of body weight) and intraperitoneal xylazine (Rompun; Mobay, Shawnee, Kan) (7 mg/kg). Transplants were placed in the subcutaneous tissues beneath the dorsal skin through a midline longitudinal skin incision. Incisions were closed with stainless steel surgical staples, which were removed prior to CT scanning. Each mouse received three, four, or five transplants. The number of transplants was determined on the basis of the number of cells available on the day that the cells were ready for transplantation. Thirty mice were given 120 transplants. The number of transplants of bone marrow stromal cells from healthy donors, patients with fibrous dysplasia of bone and McCune-Albright syndrome, patients with aplastic anemia, and patients with myelodysplasia were 51, 38, 27, and four, respectively. The mice were sacrificed at 8 weeks after surgery by using inhaled CO_2, and their transplants were harvested.

The transplants were fixed in 4% phosphate-buffered formalin freshly prepared from paraformaldehyde. After overnight fixation at 4°C, the transplants were suspended in phosphate-buffered saline. Within 3 days of harvest, all transplants were imaged in a manner described later. After imaging, transplants were prepared for embedding and sectioning. All but 12 of the 120 transplants were completely demineralized prior to embedding in buffered 10% ethylenediaminetetraacetic acid, or EDTA. Each disk-shaped transplant, measuring approximately 8 mm in diameter, was divided into four pieces by using three parallel cuts. These pieces were embedded in paraffin so that their largest cut surfaces were sectioned. A set of such sections was obtained from each transplant. Sections were deparaffinized, hydrated, and stained with hematoxylin-eosin. For 12 of the transplants, a portion of the transplant was embedded and sectioned without demineralization to assess the degree of osteomalacia in the transplant. The number of transplants undergoing such processing was limited because of the high cost. After fixation and imaging, these 12 transplants were washed with phosphate-buffered saline, placed in 70% ethyl alcohol, divided into three pieces with two parallel cuts, and embedded in methyl methacrylate so that their largest cut surfaces were sectioned first. Five-micrometer-thick sections were obtained and stained with Goldner modified trichrome.

All 120 transplants were imaged ex vivo. Because our ultimate aim was to demonstrate the feasibility of in situ evaluation of transplants, we also sought to confirm that transplants exhibited the same BMD both before and after harvest and that the harvesting and processing of the transplants did not affect their BMD. For this reason, two additional mice with 12 transplants were imaged immediately prior to sacrifice, and the BMD of each of their transplants was calculated (in situ BMD). The transplants were then harvested, fixed, imaged, and analyzed to determine the ex vivo BMD. The in situ and ex vivo BMD values for each transplant were compared with a paired *t* test (InStat, GraphPad, San Diego, Calif, and SAS, SAS Institute, Cary, NC).

Transplant Imaging and Estimation of BMD

Transplant sections were individually placed in separate wells of 48-well culture plates. Plates underwent CT (CTI; GE Medical Systems, Milwaukee, Wis) with 80 kVp, 200 mA, and section thickness of 1 mm. The scan and display fields of view were set to the finest values of the instrument, 25.0 and 9.6 cm, respectively. Images were reconstructed with the bone algorithm. Each scan included a phantom (Siemens Medical Systems, Iselin, NJ). This phantom contained only two densities, 0 and 200 mg/cm^3 K_2HPO_4; it was used in place of the much larger clinical-grade five-density phantom (Mindways Software, South San Francisco,

Semiquantitative Scale for Estimation of Bone Formation

Score	Extent of Bone in Transplant
0	No bone evident
1	Minimal bone evident (one trabecula per section)
2	Low bone formation, occupying only a small portion of the section
3	Moderate bone formation, occupying a substantial portion but less than one-half of the section
4	Abundant bone formation, occupying greater than one-half of the section

Calif) because the small phantom could be completely accommodated in each image section.

The BMD of each image section of each transplant was obtained (QCT Pro, version 2.0.3; Mindways Software, South San Francisco, Calif) with a personal computer (XPS R450; Dell Computer, Round Rock, Tex). BMD values were expressed in milligrams per cubic centimeter of K_2HPO_4 in distilled water, where a BMD of zero corresponded to the density of distilled water alone (no additional K_2HPO_4) and a BMD greater than 0 corresponded to nonaerated biologic tissue. Each transplant was represented by four to eight sections, each 1 mm thick and bounded by an oval region of interest. The software provided the regions of interest, while the investigator determined the size and shape. In each image of a transplant, the region of interest was adjusted to match the size and shape of the transplant, which was also typically oval in cross section. In situations where the transplants were not precisely oval, the region of interest was applied to the center of the transplant. Because the region of interest and the transplant silhouette were well matched to each other, the region of interest encompassed nearly the entire (>90%) transplant section in each image. Regions of interest ranged in size from 10 to 15 mm^2. The BMD values for all sections of a transplant were pooled, and the mean of these individual BMD values was used as the overall BMD value for the transplant. All BMD values were calculated by the primary author (M.H.M.), who was blinded to the bone scores of the transplants.

Estimates of Bone Formation and Comparison with BMD

The hematoxylin-eosin–stained sections were examined histologically, and the extent of bone in each transplant was scored on a semiquantitative scale by three independent blinded observers (including M.H.M., S.A.K.) in a manner similar to that described previously (23). Each observer was an investigator in our laboratory who had been trained to evaluate the histologic characteristics of the transplants. Transplants were scored on a scale of zero to 4; a score of zero corresponded to no bone formation, while a score of 4 corresponded to abundant bone formation that occupied more than one-half of the section (Table, Fig 1). The intraclass correlation coefficient was derived for the examiners to evaluate interexaminer reliability. The bone score for each transplant was the mean of the bone formation scores for the three observers (rounded to the nearest integer).

The association between clinical bone score and BMD was investigated. BMD was statistically modeled as a function of clinical bone score by means of linear regression analysis that involved a correlated error structure. Patients and animals were included as random effects. Separately, a two-way mixed effect analysis of variance model was used to compare mean BMD scores for transplants with poor bone scores (scores of 0 to 2) with those with good bone scores (scores of 3 or 4) and for four patient diagnostic classes. Random effects for patients and animals were included in the modeling of the errors structure. Statistical analyses were conducted (Excel, Microsoft, Redmond, Wash, and SAS ["proc mixed" function], SAS Institute).

Empiric receiver operating characteristic (ROC) curves were used to determine the optimum BMD thresholds to distinguish *(a)* no bone formation (bone score of zero) from any bone formation (bone score of more than 0), and *(b)* poor bone formation (bone score of 0 or 1) from appreciable bone formation (bone score of 3 or 4). To achieve this, we graphed the true-positive rate (sensitivity) over the false-positive rate (1 − specificity), with each observed BMD value as a potential cut point or threshold. We then found the straight line with positive unit slope that is tangent to the ROC curve. The point of tangency of this line to the curve determined the sensitivity and specificity that yielded maximum sum of sensitivity plus specificity (23–26). The area under each of the ROC curves was also calculated (SAS ["proc logistic" function]; SAS Institute).

Estimates of Mineralization and Comparison with BMD

We suspected that a number of transplants contained osteomalacic bone because this had been seen episodically during examination of undemineralized sections. Owing to cost constraints, only a fraction (12 transplants) of the 120 transplants examined in this study underwent concomitant undemineralized processing. A section from each transplant that had been embedded in methyl methacrylate was digitized (Axioplan2 microscope; Carl Zeiss Mikroskopie, Göttingen, Germany) with a ×1.25 objective by using a digital microscope camera (Polaroid, Cambridge, Mass). After staining with Goldner modified trichrome, normal well-mineralized bone could be identified by its green hue, while osteomalacic bone was red (Fig 1). The total amount of normal (green) and osteomalacic (red) bone was measured (Photoshop, version 5.0; Adobe Systems, San Jose, Calif). The proportion of normal bone to all bone in the transplant was calculated by using the following relationship: percentage of normal bone = 100 × (area of normal bone)/(area of normal bone + area of osteomalacic bone). A comparison was made between the percentage of normal bone and the BMD for these transplants by means of linear regression with correlated error structure.

RESULTS

One hundred twenty transplants were evaluated. Bone marrow stromal cells were harvested from 22 donors (age range, 1.5–69.0 years. Forty-five transplants were obtained from male patients, 71 were obtained from female patients, and four were obtained from patients whose sex was not recorded. Fifty-eight transplants came from healthy donors, 37 from patients with fibrous dysplasia of bone and McCune-Albright syndrome, 21 from patients with aplastic anemia, and four from patients with myelodysplasia. The amount of bone formation in the transplants ranged from a bone score of zero to a score of 4; the frequency of implants with the respective bone scores is presented in Figure 2. The 120 transplants were sorted into five groups that corresponded to one of the five bone

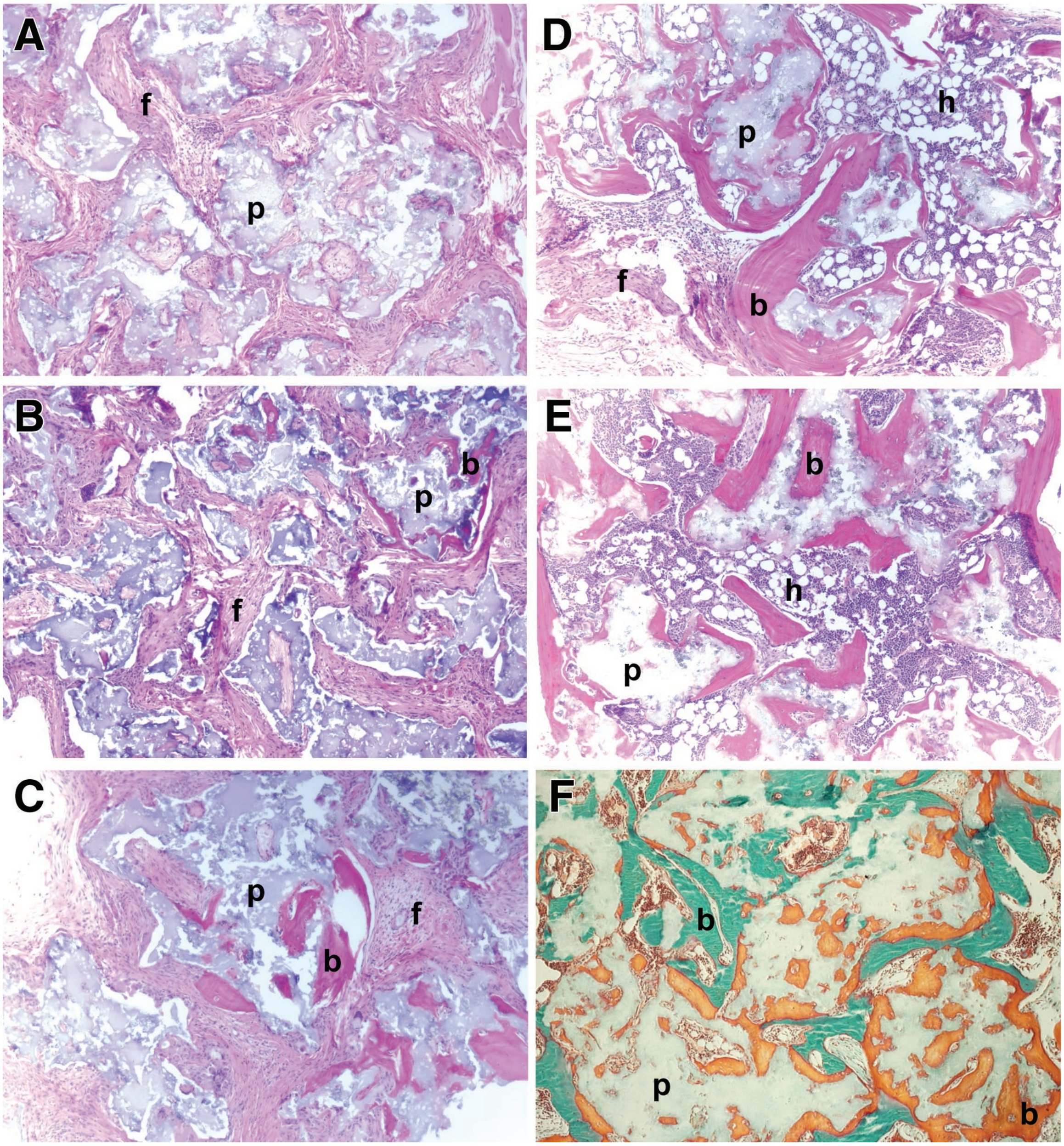

Figure 1. Photomicrographs show sections of HA-TCP and bone marrow stromal cell transplants with varying amounts of bone formation. *A–E,* Paraffin embedding following demineralization. (Hematoxylin-eosin stain; original magnification, ×50.) *A,* Bone score of 0 (no bone formation present). Rather, particles are widely separated by connective tissue. *B,* Bone score of 1 (only one bone trabecula present). *C,* Bone score of 2 (weak bone formation, with only a few trabeculae present). New bone does not bridge adjacent particles. *D,* Bone score of 3 (bone formation is appreciable but less than one-half of the transplant). *E,* Bone score of 4 (abundant bone formation). Bone bridges adjacent particles. *F,* Methyl methacrylate embedding without demineralization. Transplant exemplifies the difference between areas of normal (green) versus osteomalacic (red) bone. (Goldner modified trichrome stain; original magnification, ×50.) *b* = bone, *f* = fibrous connective tissue, *h* = hematopoietic tissue, *p* = particle.

scores (Figs 2, 3). Forty-six transplants showed no or poor bone formation (bone scores of 0 to 2), while the remaining 74 transplants showed appreciable amounts of bone formation (bone scores of 3 or 4).

The intraclass correlation coefficient was 0.92 for the 120 bone scores given by the three observers. Their scores agreed for 108 implants. For the other 12 transplants, one reviewer gave a score that was one unit higher or lower than the scores given by the other two reviewers. The summary statistic for the clinical bone score was the average score, rounded to the nearest integer (in this case essentially equivalent to the median of the three scores).

BMD values of the transplants ranged from 425 to 877 mg/cm^3 K_2HPO_4 (Fig 3). We modeled the BMD as a function of clinical bone score by means of linear

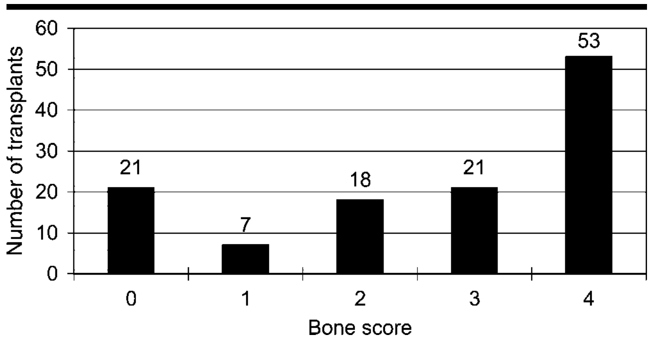

Figure 2. Bar graph shows bone formation among the 120 transplants, with bone scores from 0 (no bone formation) to 4 (extensive bone formation).

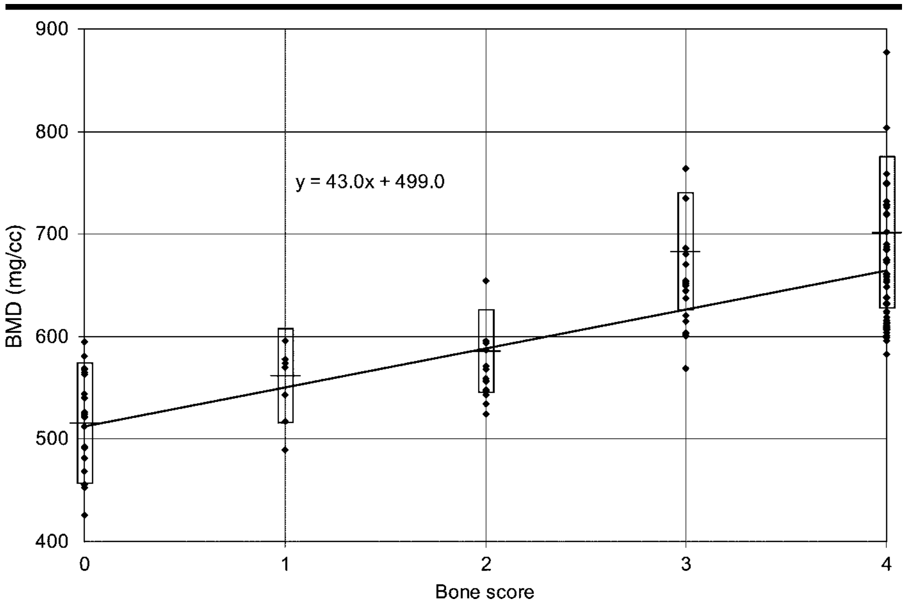

Figure 3. Scatterplot shows raw BMD values among the 120 transplants, sorted by bone score. BMD increased linearly with increasing bone score. Error boxes indicate mean BMD ± 1 SD.

regression with a correlated error structure that reflected correlation among implants from the same donor and those placed in the same animal (no covariates included). A significant ($P < .001$) positive trend in BMD was detected as a function of clinical bone score. The estimated relationship is given as BMD = 43.0 · bone score + 499.0.

BMD could be used to distinguish between no bone formation and any level of bone formation. When a BMD of 569 mg/cm^3 K_2HPO_4 was used as a threshold between the absence (bone score of 0) and presence (bone score of more than 0) of bone formation, quantitative CT had sensitivity and specificity of 85% and 86%, respectively (Fig 4a). Note that the ROC curve is nearly parallel to the tangent line in this portion of the graph. Nonetheless, a threshold of 569 represents maximization of the sum of sensitivity and specificity, while parity is maintained between these two parameters. The area under this ROC curve was 0.90. When a BMD of 600 mg/cm^3 K_2HPO_4 was used as a threshold between poor (bone score < 3) bone formation and appreciable (bone score ≥ 3) bone formation, quantitative CT had sensitivity and specificity of 99% and 96%, respectively (Fig 4b). The area under this second ROC curve was 0.97.

The 120 transplants were also analyzed according to patient diagnosis and a dichotomized bone score (Fig 5). A two-way mixed effect analysis of variance with correlated error structure ("patients in diagnostic class" and "animal" were included as random effects) was performed (SAS ["proc mixed" function]; SAS Institute) on the BMD scores as a function of a dichotomous clinical bone score and patient diagnosis. A clear consistent increase in mean BMD was observed among transplants with a good bone score (score of 3 or 4) in comparison to that with transplants with poor bone scores (score of 0 to 2). The mean BMD was calculated separately for each patient diagnostic classification ($P < .001$ for each diagnosis, except $P = .0188$ for patients with myelodysplasia, with no interaction detectable). These P values were obtained from individual differences with no adjustment for multiple tests performed.

When normal transplants were compared with osteomalacic transplants, BMD varied in proportion to the percentage of normal bone in the transplant. This relationship was valid among transplants representing all levels of bone formation. Twelve transplants underwent processing without demineralization. Of these, one had a bone score of 1, two had a score of 2, five had a score of 3, and four had a score of 4. The percentage of normal bone ranged from 17% to 97% (Fig 6). When the percentage of normal bone was compared with BMD for these 12 transplants, a Pearson correlation coefficient of $r = 0.76$ was derived.

To demonstrate that the BMD calculations were unaffected by transplant harvest, 12 transplants from two additional mice were imaged both in situ and in vivo. In situ measurements were obtained from CT scans obtained immediately after the mice were sacrificed. After transplant harvest and overnight fixation, the transplants alone were imaged and analyzed to derive ex vivo BMD values. Results of a paired t test showed that the in situ and ex vivo values were not significantly different ($P = .986$). In situ BMD values ranged from 590 to 863 mg/cm^3 K_2HPO_4 (SD, 88.33; standard error of the mean, 25.5), while ex vivo values ranged from 576 to 873 mg/cm^3 K_2HPO_4 (SD, 89.23; standard error of the mean, 25.8).

DISCUSSION

HA-TCP particles are becoming an increasingly important matrix for bone reconstruction and tissue engineering (27–35). While their mineral content, density, and three-dimensional properties have made them particularly suitable in the bone microenvironment, these characteristics have increased the difficulty of evaluating new bone formation radiographically. Radiologists and sur-

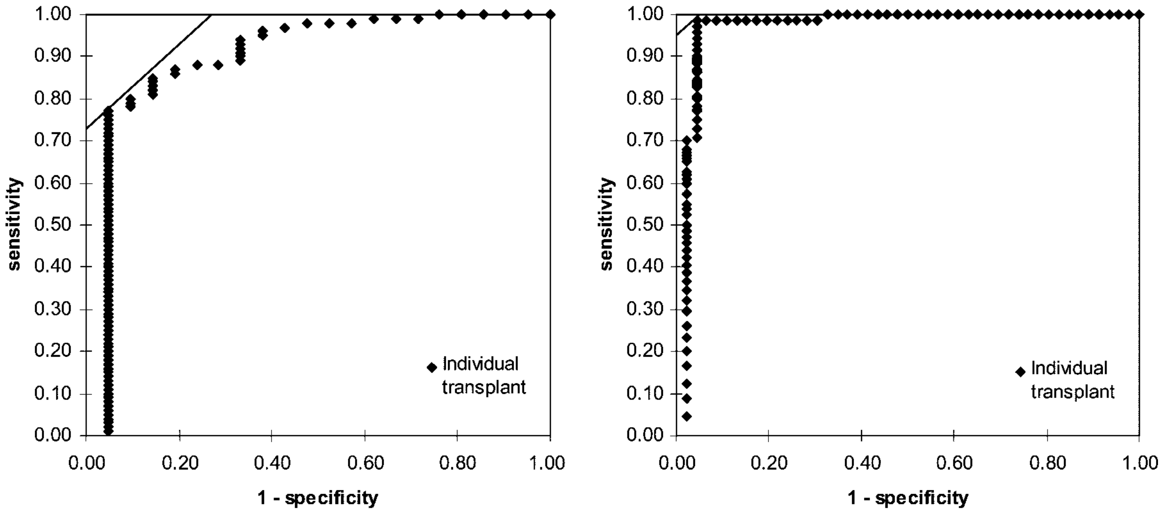

a. b.

Figure 4. **(a)** ROC curve distinguishes no bone formation from any bone formation. Sensitivity and specificity of 85% and 86%, respectively, represent the highest balanced combination of these two values. **(b)** ROC curve distinguishes poor bone formation from appreciable bone formation. Sensitivity and specificity of 99% and 96%, respectively, represent the highest combination of these two values.

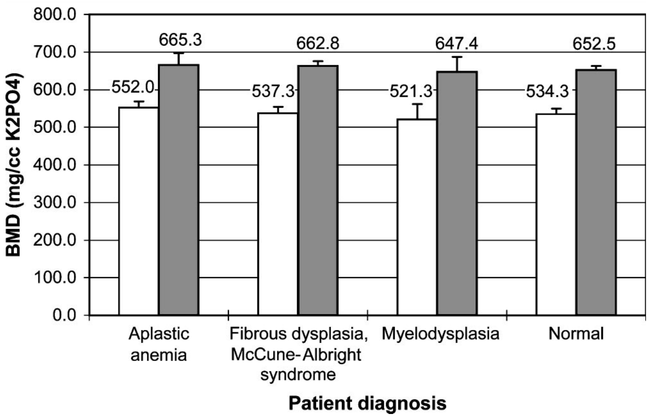

Figure 5. Bar graph shows the difference in BMD between transplants with bone scores of 0 to 2 (white bars) and those with bone scores of 3–4 (gray bars) regardless of whether the donor had normal bone or bone disease.

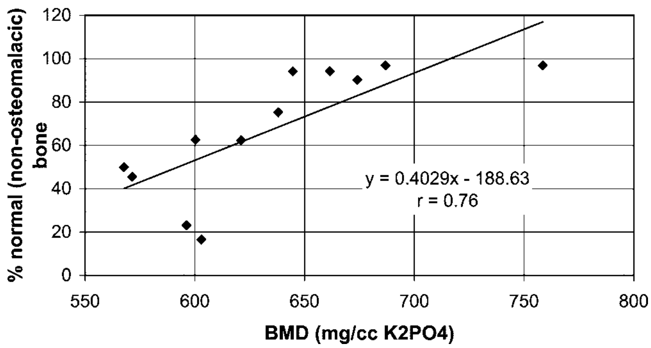

Figure 6. Scatterplot shows results in 12 transplants processed without demineralization. The proportion of normal nonosteomalacic bone increased in proportion to BMD.

geons have evaluated HA-TCP transplants with indirect measures, including callus formation at the interface between the construct and adjacent normal bone. While such radiographic features are helpful, they do not provide information about the nature of the new tissue in the interior of the construct. In addition, radiographs have limited utility in the evaluation of spatially complex reconstructions that do not permit a clear view of the construct-bone interface. CT scanning, combined with attenuation measurements in Hounsfield units, can theoretically depict differences in density between transplants that have formed bone and those that have not. To our knowledge, however, no previously published study has attempted to do so. This is most likely because a rigorous evaluation would require a comparison of radiographic results with those at comprehensive tissue histologic examination. To move a step beyond the use of Hounsfield units, quantitative CT techniques, including the placement of a standard phantom in each image, would permit standardization across different scanners and at different time points.

In the current study, the transplantation system involved cultured human osteogenic bone marrow stromal cells combined with HA-TCP particles. After subcutaneous transplantation into mice, transplants formed a mature bone structure in 8 weeks. The extent of bone formation varied widely, permitting a rigorous comparison of a variety of transplants. Since this study design is complex, involving multiple implants for each donor and recipient mouse, it was necessary to model the correlation structure in each donor and each recipient. All transplants were harvested and underwent both CT with BMD evaluation and histologic examination in a blinded fashion. The BMD among transplants with little or no new bone formation was significantly less than that among transplants with appreciable amounts of bone formation. The relationship between BMD and bone formation held true whether the bone marrow stromal cells came from healthy donors or patients with fibrous dysplasia of bone, McCune-Al-

Radiology

bright syndrome, aplastic anemia, or myelodysplasia. In addition, a BMD of 600 mg/cm^3 K_2HPO_4 served as a threshold to distinguish a transplant with poor bone formation from one with good bone formation.

The interval between transplantation and harvest (8 weeks) was carefully selected. We envisioned that clinical use of this scanning technique would include the early evaluation of transplant sites to inform surgeons at an early postoperative stage whether or not bone was forming successfully. An 8-week time point was chosen because it represents the standard time for bone marrow stromal cells and HA-TCP transplants to show bone formation. Care was also taken to specifically use a clinical CT scanner rather than a CT unit used for investigational purposes. While a research CT scanner would undoubtedly have provided much better resolution and a finer section thickness in our small transplants, it was important to us to demonstrate the feasibility of using quantitative CT with clinically appropriate equipment and settings.

A semiquantitative scale of bone formation was used in the current study for comparison to BMD. Previously when the bone scores on this scale were compared with histomorphometric measurements in tissue sections, a correlation was observed between the bone score and the square root of the fraction of bone area to total transplant area (r = 0.973) (36). In that study, bone scores of 0, 1, 2, 3, and 4 correlated with fractional bone areas of 0, 1%, 3%, 8%, and 14%, respectively. Poor bone formation was characterized by a fractional bone area of 3% or less, while appreciable bone formation was characterized by a fractional bone area of 8% or more. Thus, the differences in BMD noted between transplants with poor and those with appreciable bone formation paralleled significant differences in the fraction of bone area to total transplant area.

Bone marrow stromal cell transplants from both healthy volunteers and patients with bone diseases were used in the current study. Mature human bone marrow stromal cell transplants replicate many of the histologic features of the donor tissue from which they are derived. Transplants from patients with fibrous dysplasia of bone and McCune-Albright syndrome, for instance, demonstrate woven bone, cells and collagen bundles oriented perpendicular to the bone surface, and hyperosteocytic bone. Such transplants are characteristic of dystrophic bone from patients with fibrous dysplasia of bone and McCune-Albright syndrome (37). These findings have potential clinical relevance; they provide a rationale for the use of BMD measurements not only in healthy patients but also in those with skeletal diseases.

We also determined that quantitative CT for the determination of BMD was not influenced by the harvesting and fixation of the transplants. Quantitative CT will be most clinically useful in the analysis of constructs in situ. In the current study, the majority of mice could not be sacrificed at a time when the CT scanner was available for research use. As a result, transplants were often imaged the day following harvest. However, results at quantitative CT analysis of 12 transplants both before and after harvest confirmed that BMD values did not vary significantly.

Practical application: Until now, no method existed for noninvasive determination of the extent of new bone formation in transplants containing HA-TCP because new bone is overshadowed by preexisting mineral. Surgeons and dentists have relied on biopsies to evaluate the success of these transplants. Our results indicate that the BMD of transplants with bone formation is significantly higher than that of transplants without bone formation. Consequently, quantitative CT can be used to estimate the extent of new bone formation in HA-TCP–based transplants. It has the potential for noninvasive evaluation of the success of such bone grafting materials.

Acknowledgments: The authors thank Zimmer (Warsaw, Ind) for the gift of HA-TCP; Mindways Software (South San Francisco, Calif) for the gift of hydroxyapatite/tricalcium phosphate; Chris Cann, PhD, for technical assistance and the gift of a phantom (Mindways Software); and Dennis Johnson, BS, David Williams, BS, and Ronald Norman, RT (Department of Radiology, Clinical Center, National Institutes of Health, Bethesda, Md) for assistance with imaging.

References

1. Ono I, Gunji H, Kaneko F, Numazawa S, Kodama N, Yoza S. Treatment of extensive cranial bone defects using computer-designed hydroxyapatite ceramics and periosteal flaps. Plast Reconstr Surg 1993; 92:819–830.
2. Yamashima T. Cranioplasty with hydroxylapatite ceramic plates that can easily be trimmed during surgery: a preliminary report. Acta Neurochir (Wien) 1989; 96:149–153.
3. Fortunato G, Marini E, Valdinucci F, Bonucci E. Long-term results of hydroxyapatite-fibrin glue implantation in plastic and reconstructive craniofacial surgery. J Craniomaxillofac Surg 1997; 25:124–135.
4. Bonucci E, Marini E, Valdinucci F, Fortunato G. Osteogenic response to hydroxyapatite-fibrin implants in maxillofacial bone defects. Eur J Oral Sci 1997; 105:557–561.
5. Byrd HS, Hobar PC, Shewmake K. Augmentation of the craniofacial skeleton with porous hydroxyapatite granules. Plast Reconstr Surg 1993; 91:15–26.
6. Choi SH, Levy ML, McComb JG. A method of cranioplasty using coralline hydroxyapatite. Pediatr Neurosurg 1998; 29:324–327.
7. Mattelin W, Albers FW. Reconstruction of defects in the anterior skull base with calcium phosphate ceramics. Acta Otorhinolaryngol Belg 1993; 47:335–338.
8. Matukas VJ, Clanton JT, Langford KH, Aronin PA. Hydroxylapatite: an adjunct to cranial bone grafting. J Neurosurg 1988; 69:514–517.
9. Nakajima T, Yoshimura Y, Nakanishi Y, Kanno T, Sano H, Kamei Y. Anterior cranial base reconstruction using a hydroxyapatite-tricalciumphosphate composite (Ceratite) as a bone substitute. J Craniomaxillofac Surg 1995; 23:64–67.
10. Ono I, Tateshita T, Satou M, Sasaki T, Matsumoto M, Kodama N. Treatment of large complex cranial bone defects by using hydroxyapatite ceramic implants. Plast Reconstr Surg 1999; 104:339–349.
11. Pompili A, Caroli F, Carpanese L, et al. Cranioplasty performed with a new osteoconductive osteoinducing hydroxyapatite-derived material. J Neurosurg 1998; 89:236–242.
12. Yamashima T. Reconstruction of surgical skull defects with hydroxylapatite ceramic buttons and granules. Acta Neurochir (Wien) 1988; 90:157–162.
13. Weissman JL, Snyderman CH, Hirsch BE. Hydroxyapatite cement to repair skull base defects: radiologic appearance. AJNR Am J Neuroradiol 1996; 17:1569–1574.
14. Waite PD, Morawetz RB, Zeiger HE, Pincock JL. Reconstruction of cranial defects with porous hydroxylapatite blocks. Neurosurgery 1989; 25:214–217.
15. Benque E, Zahedi S, Brocard D, Marin P, Brunel G, Elharar F. Tomodensitometric and histologic evaluation of the combined use of a collagen membrane and a hydroxyapatite spacer for guided bone regeneration: a clinical report. Int J Oral Maxillofac Implants 1999; 14:258–264.
16. Ito M, Hayashi K, Uetani M, et al. Bone mineral and other bone components in vertebrae evaluated by QCT and MRI. Skeletal Radiol 1993; 22:109–113.
17. Zgliczynski S, Szulc P, Slowinska-Srednicka J, et al. Measurement of bone mineral density (BMD) with quantitative computed tomography (QCT) in postmenopausal osteoporosis: effect of estrogen. Endokrynol Pol 1992; 43:350–357.
18. Markel MD, Wikenheiser MA, Morin RL, Lewallen DG, Chao EY. Quantification of bone healing: comparison of QCT, SPA, MRI, and DEXA in dog osteotomies. Acta Orthop Scand 1990; 61:487–498.
19. Muller A, Ruegsegger E, Ruegsegger P. Peripheral QCT: a low-risk procedure to identify women predisposed to osteoporosis. Phys Med Biol 1989; 34:741–749.
20. Gluer CC, Reiser UJ, Davis CA, Rutt BK, Genant HK. Vertebral mineral determination by quantitative computed tomography (QCT): accuracy of single

and dual energy measurements. J Comput Assist Tomogr 1988; 12:242–258.
21. Ito M, Matsumoto T, Enomoto H, Tsurusaki K, Hayashi K. Effect of nonweight bearing on tibial bone density measured by QCT in patients with hip surgery. J Bone Miner Metab 1999; 17:45–50.
22. Kuznetsov SA, Krebsbach PH, Satomura K, et al. Single-colony derived strains of human marrow stromal fibroblasts form bone after transplantation in vivo. J Bone Miner Res 1997; 12:1335–1347.
23. Hanley JA. Receiver operating characteristic (ROC) methodology: the state of the art. Crit Rev Diagn Imaging 1989; 29: 307–335.
24. Farr BM, Shapiro DE. Diagnostic tests: distinguishing good tests from bad and even ugly ones. Infect Control Hosp Epidemiol 2000; 21:278–284.
25. Greiner M, Pfeiffer D, Smith RD. Principles and practical application of the receiver-operating characteristic analysis for diagnostic tests. Prev Vet Med 2000; 45:23–41.
26. Centor RM. Signal detectability: the use of ROC curves and their analyses. Med Decis Making 1991; 11:102–106.
27. Williams JK, Ellenbogen RG, Gruss JS. State of the art in craniofacial surgery: nonsyndromic craniosynostosis. Cleft Palate Craniofac J 1999; 36:471–485.
28. Cornell CN, Lane JM. Current understanding of osteoconduction in bone regeneration. Clin Orthop 1998; suppl 335: S267–S273.
29. Fulmer NL, Bussard GM, Gampper TJ, Edlich RF. Anorganic bovine bone and analogs of bone mineral as implants for craniofacial surgery: a literature review. J Long Term Eff Med Implants 1998; 8:69–78.
30. Hirano S, Shoji K, Kojima H, Omori K. Use of hydroxyapatite for reconstruction after surgical removal of intraosseous hemangioma in the zygomatic bone. Plast Reconstr Surg 1997; 100:86–90.
31. Black B, Kelly S. Mastoidectomy reconstruction: management of the high facial ridge using hydroxylapatite implants. Am J Otol 1994; 15:785–792.
32. Spector M. Anorganic bovine bone and ceramic analogs of bone mineral as implants to facilitate bone regeneration. Clin Plast Surg 1994; 21:437–444.
33. Zeltser C, Masella R, Cholewa J, Mercier P. Surgical and prosthodontic residual ridge reconstruction with hydroxyapatite. J Prosthet Dent 1989; 62:441–448.
34. el Deeb ME, Tompach PC, Morstad AT. Porous hydroxylapatite granules and blocks as alveolar ridge augmentation materials: a preliminary report. J Oral Maxillofac Surg 1988; 46:955–970.
35. Frame JW, Brady CL. The versatility of hydroxyapatite blocks in maxillofacial surgery. Br J Oral Maxillofac Surg 1987; 25:452–464.
36. Mankani MH, Kuznetsov SA, Fowler B, Kingman A, Robey PG. In vivo bone formation by human bone marrow stromal cells: effect of carrier particle size and shape. Biotechnol Bioeng 2001; 72:96–107.
37. Bianco P, Kuznetsov SA, Riminucci M, Fisher LW, Spiegel AM, Robey PG. Reproduction of human fibrous dysplasia of bone in immunocompromised mice by transplanted mosaics of normal and Gsalpha-mutated skeletal progenitor cells. J Clin Invest 1998; 101:1737–1744.